Single-Particle Mobility Edge in a One-Dimensional Quasiperiodic Optical Lattice

Henrik P. Lüschen,[1,2] Sebastian Scherg,[1,2] Thomas Kohlert,[1,2] Michael Schreiber,[1,2]
Pranjal Bordia,[1,2] Xiao Li,[3] S. Das Sarma,[3] and Immanuel Bloch[1,2,*]
[1]Fakultät für Physik, Ludwig-Maximilians-Universität München, Schellingstraße 4, 80799 Munich, Germany
[2]Max-Planck-Institut für Quantenoptik, Hans-Kopfermann-Straße 1, 85748 Garching, Germany
[3]Condensed Matter Theory Center and Joint Quantum Institute, University of Maryland, College Park, Maryland 20742-4111, USA

(Received 15 September 2017; published 19 April 2018)

A single-particle mobility edge (SPME) marks a critical energy separating extended from localized states in a quantum system. In one-dimensional systems with uncorrelated disorder, a SPME cannot exist, since all single-particle states localize for arbitrarily weak disorder strengths. However, in a quasiperiodic system, the localization transition can occur at a finite detuning strength and SPMEs become possible. In this Letter, we find experimental evidence for the existence of such a SPME in a one-dimensional quasiperiodic optical lattice. Specifically, we find a regime where extended and localized single-particle states coexist, in good agreement with theoretical simulations, which predict a SPME in this regime.

DOI: 10.1103/PhysRevLett.120.160404

Introduction.—In the presence of uncorrelated disorder, noninteracting systems can undergo Anderson localization [1], resulting in an exponential localization of wave functions. In one and two dimensions, all eigenstates already localize at infinitesimal disorder strengths. In three dimensions, however, the transition occurs at a finite disorder strength [2] and not all eigenstates need to localize at the same critical value. Instead, localized and extended states can coexist at different energies, which is the most prominent example of a so-called single-particle mobility edge (SPME) [2,3]: a critical energy separating localized from extended eigenstates. In three dimensions, this phenomenon was, among other systems (see Ref. [3] for a review), observed in recent experiments with ultracold atoms [4–6], but the interpretation of the results has remained challenging [7]. While one-dimensional systems with uncorrelated disorder rigorously do not exhibit a SPME, as all states are localized for arbitrarily weak disorder strengths [8], a related quantity called "effective mobility edge" has been identified in one-dimensional speckle potentials [9]. This effective mobility edge emerges due to a finite correlation length in the speckle potential and separates exponentially from algebraically localized states [9,10], as compared to localized from extended states in systems with a true mobility edge.

For quasiperiodic potentials, it is possible to construct models that do exhibit exact SPMEs even in one dimension [11–23]. Until now, however, their realization has remained out of reach for experiments in spite of the growing number of theoretical proposals during the last 30 years. Recently, however, the existence of a SPME was predicted for the superposition of two optical lattices with incommensurate wavelengths [24,25]. For shallower lattices, the SPME is present in an intermediate phase, which separates the fully extended from the fully localized phase. At deeper lattice depths, where the nearest-neighbor tight-binding limit is approached, the intermediate phase shrinks and eventually vanishes [25]. In this limit, the system maps onto the Aubry-André Hamiltonian [26–30], which does not display a SPME.

In this Letter, we report on the direct experimental observation of this intermediate phase in very good agreement with the theoretical predictions [25]. The good agreement implies the existence of a SPME in the system, even though the critical energy itself is not directly accessible in our experiment. We probe the intermediate phase of the bichromatic incommensurate lattice by monitoring the time evolution of an initial charge-density wave (CDW) state, as illustrated in Fig. 1. The presence of *localized* states is indicated by a persisting CDW pattern for long evolution times, which is quantified via a finite density imbalance between even and odd sites $\mathcal{I} = (N_e - N_o)/(N_e + N_o)$. Here, N_e (N_o) denote the atom number on even (odd) sites, respectively. The presence of *extended* states can be probed by monitoring the global size of the atom cloud $\sigma(t)$. A continuously growing expansion $\mathcal{E} \sim [\sigma(t) - \sigma(0)]$ shows the presence of extended states. The intermediate phase is thus characterized by simultaneously finite values of both $\mathcal{I}$ and $\mathcal{E}$, which directly shows the coexistence of localized and extended states. Note, that the two quantities $\mathcal{I}$ and $\mathcal{E}$ are complementary in the sense that the imbalance is not sensitive to the presence of few extended states and the expansion is not sensitive to the presence of few localized states. Both quantities have been successfully utilized to study localization properties in earlier experiments [27,28,30]. Crucially, in this Letter, we utilize both observables simultaneously in order to detect the presence of the intermediate phase. When both

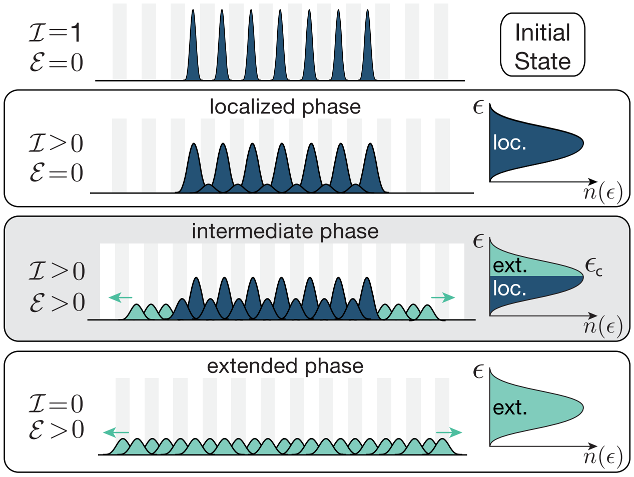

FIG. 1. Schematics of the experiment. Schematic illustration of the initial CDW state and the states reached after time evolution in the localized, intermediate, and extended phase, respectively. The presence of localized states is marked by a persisting CDW order ($\mathcal{I} > 0$), while the presence of extended states is marked by an increase of the cloud size over time ($\mathcal{E} > 0$). In the intermediate phase, extended and localized states coexist at different energies and lead to simultaneously finite values of both $\mathcal{I} > 0$ and $\mathcal{E} > 0$. As is illustrated in the diagrams of the density of states $n(\epsilon)$, they are separated by a critical energy ϵ_c [25], called the mobility edge.

indicators are finite, this implies the coexistence of both extended and localized states, which is the key ingredient of this Letter.

Experiment.—In the experiment, the bichromatic optical lattice is realized via the superposition of a $\lambda_p \approx 532.2$ nm "primary" lattice and a weaker incommensurate $\lambda_d \approx 738.2$ nm "detuning" lattice at respective depths of V_p and V_d. Deep lattices along the orthogonal directions split the system into an array of one-dimensional tubes. The system is well described by the one-dimensional Hamiltonian

$$\hat{H} = -\frac{\hbar^2}{2m}\frac{d^2}{dx^2} + \frac{V_p}{2}\cos(2k_p x) + \frac{V_d}{2}\cos(2k_d x + \phi), \quad (1)$$

which has been studied numerically in Ref. [25]. Here, $k_i = 2\pi/\lambda_i$ $(i = p, d)$ denote the wave vectors of the two lattices, ϕ is the relative phase between them, and m is the mass of the ^{40}K atoms employed in the experiment. We start the experiments by loading a gas of 130×10^3 spin-polarized (and hence noninteracting) atoms at a temperature of $0.15T_F$, into the primary and orthogonal lattices. Here, T_F denotes the Fermi temperature in the dipole trap. Adding a superlattice ($\lambda_{\mathrm{sup}} = 1064$ nm) to the primary lattice, the initial CDW state is created [30]. The time evolution is initiated by suddenly switching off the superlattice and quenching the primary and detuning lattices to their respective values. This quench results in the occupation of single-particle states throughout the entire energy spectrum. After the time evolution, the imbalance $\mathcal{I}$ is extracted using a superlattice band-mapping technique [30,31]. As in previous experimental works [32,33], the size of the cloud σ is determined from *in situ* pictures and characterized by the full width at half maximum (FWHM). The expansion is calculated as $\mathcal{E} = A \times [\sigma(t) - \sigma(0)]$, where $A = 0.01/\text{site}$ is a constant scaling factor designed to enable a direct comparison of $\mathcal{E}$ and $\mathcal{I}$ on the same scale.

We compare the experimental observables to numerical simulations. While the imbalance is directly simulated as in the experiment, the expansion is quantified via the edge density $\mathcal{D}$, which is a more direct measure of the extended states in theoretical simulations [25,34]. It is calculated by initially populating the eigenstates of the center third of the system before quenching to the full system. After time evolution, the edge density is calculated as $\mathcal{D} = 1 - N_c/N$, where N is the total particle number and N_c is the particle number in the originally populated center third of the system. It therefore gives the fraction of particles that leaves the originally populated center.

Expansion versus edge density.—Figure 2 compares time traces of the experimental cloud size σ and the edge density $\mathcal{D}$ in the extended, intermediate, and localized phases. We find that the two quantities indeed show a qualitatively similar behavior (see Supplemental Material [34]) in describing the expansion of the system. In the extended

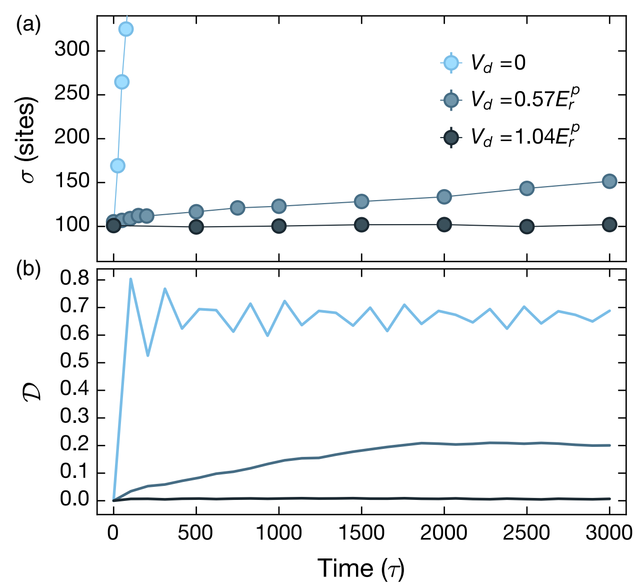

FIG. 2. Expansion versus edge density. Time evolution of the (a) experimental FWHM cloud size σ and (b) edge density $\mathcal{D}$ obtained from numerical simulations at a primary lattice depth of $V_p = 4E_r^p$. Data are shown in the extended ($V_d = 0$), intermediate ($V_d = 0.57E_r^p$), and localized ($V_d = 1.04E_r^p$) phase. Here, $E_r^p = \hbar^2 k_p^2/2m$ denotes the recoil energy of the primary lattice and the tunneling time $\tau = \hbar/J$, where J denotes the nearest-neighbor tunneling rate in the primary lattice. The edge density eventually saturates due to the finite size of the simulated system.

phase, both quantities show a rapid expansion, which saturates in the numerics due to the finite size of the simulated system. In the intermediate phase, the expansion becomes dramatically slower and the numerical curve saturates to a lower value, already suggesting that not all particles are expanding. In the localized phase, neither the experiment nor the numerics show a discernible expansion.

To enable the expansion of the cloud in the experiment, any confining (or anticonfining) potential needs to be removed. This is achieved by compensating the anticonfinement of the (blue detuned) optical lattices with the confining potential of the dipole trap to create a homogeneous potential, as in Refs. [32–34]. However, the expansion dynamics in the experiment are still likely slowed down by a small residual unevenness in the potential. This is true especially in the intermediate phase, as any unevenness becomes increasingly important in the presence of the detuning lattice [34]. Still, a finite expansion remains a definite signature for the presence of extended states.

Results.—We characterize the phases of the Hamiltonian in Eq. (1) via measurements of the imbalance and the expansion for various depths of the primary and detuning lattices V_p and V_d at fixed times. Due to the extremely slow expansion dynamics found in the intermediate phase (see Fig. 2), we choose to extract the cloud sizes after evolution times of 3000τ. Such long evolution times are, however, not accessible for the imbalance, since it is much more susceptible to the effects of external baths, limiting its lifetime to about $T \sim 2000\tau$ in our case [35,36]. Therefore, we extract the imbalance after 200τ. This is a compromise of minimizing the effects of background decays, as well as

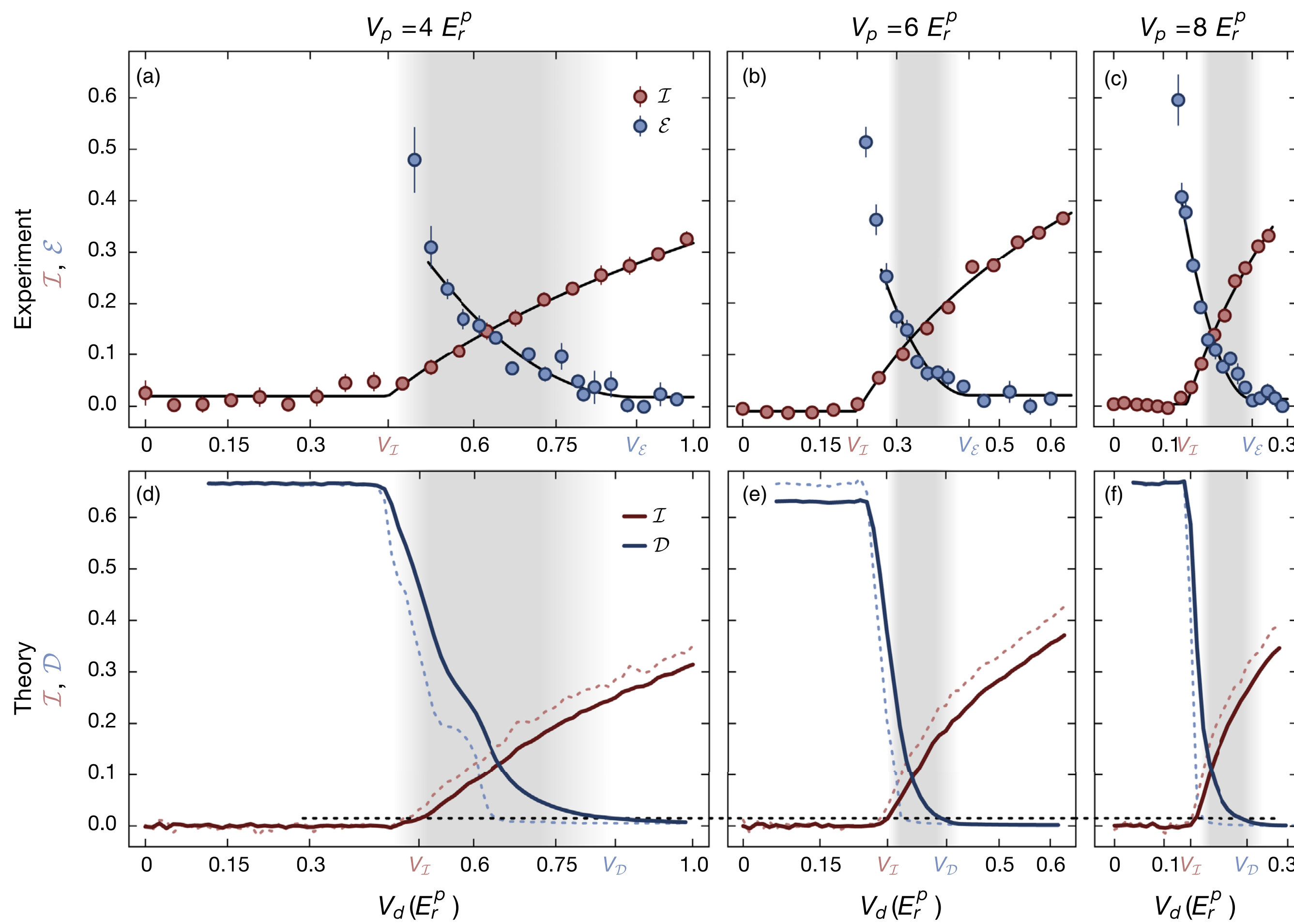

FIG. 3. Identification of the intermediate phase. (a)–(c) Imbalance $\mathcal{I}$ after 200τ and expansion $\mathcal{E}$ after 3000τ versus detuning lattice strength V_d for various depths of the primary lattice V_p. Experimental data are averaged over six disorder phases, and the error bars denote the standard error of the mean. Solid lines are fitting functions to extract the critical detuning strengths for the imbalance $V_\mathcal{I}$ and the expansion $V_\mathcal{E}$. (d)–(f) Theoretically calculated imbalance $\mathcal{I}$ and edge density $\mathcal{D}$. Solid lines include the effect of averaging over many tubes with slightly different lattice depths, as is present in the experiment. Dashed lines show the result of the calculation of only the central tube (see also Ref. [25]). The critical detuning strengths $V_\mathcal{I}$ ($V_\mathcal{D}$) are extracted as the points, where $\mathcal{I}$ ($\mathcal{D}$) crosses a value of 0.015, which is marked as the black dashed horizontal line. The gray shaded region roughly marks the intermediate phase, where both the imbalances and the expansion observables are simultaneously finite and hence indicate the coexistence of extended and localized states.

minimizing finite time errors due to slow dynamics in the intermediate phase. We note that the imbalance is an intrinsically much faster observable than the expansion, as it does not require mass transport. In the absence of slow dynamics, it typically becomes stationary after few tunneling times already [30]. Even for the slow dynamics in the intermediate phase, the imbalance extracted after 200τ gives a reasonable estimate of its long time stationary value. We have verified this by comparing the numerically calculated imbalance after 3000τ to the experimental value [34].

Measurements of $\mathcal{I}$ and $\mathcal{E}$ are shown in Figs. 3(a)–3(c). We find that at all strengths of the primary lattice, three distinct phases exist. At weak detuning lattice strengths, we always find an extended phase. It is characterized by a vanishing imbalance ($\mathcal{I} \approx 0$), which directly shows the absence of any localized states. At large detuning lattice strengths, we find a fully localized phase, which is marked by the absence of expansion ($\mathcal{E} \approx 0$). In between, a regime is found where both the imbalance and the expansion are simultaneously finite ($\mathcal{I} > 0$, $\mathcal{E} > 0$). This directly shows the coexistence of extended and localized states, which is the defining feature of the intermediate phase, in which a SPME is present [25].

We compare our experimental results to the numerical simulations performed in Ref. [25], which are illustrated as dashed lines in Figs. 3(d)–3(f). We find a good agreement between the experimental and numerically simulated imbalance. However, the theoretical edge density predicts a narrower intermediate phase than the experimental expansion. We find that this difference can be explained by an averaging over many one-dimensional systems (tubes) inherently present in the experiment [34]. Due to the finite extension of the beams creating the optical lattices, tubes on the outside of the system experience slightly lower lattice depths V_p and V_d than those in the center. The solid lines in Figs. 3(d)–3(f) show the numerical results including this effect. While the imbalance is only affected qualitatively, the edge density now also shows expansion up to larger detuning lattice depths as in the experiment. The stronger effect of averaging over the tubes on the edge density as compared to the imbalance is due to the first localized states emerging in the central tube with the highest lattice depths, while the last extended states vanish on the outside tubes, where the lattice depths are the lowest. The theoretical prediction of the intermediate phase including the averaging over many tubes is in very good agreement with the experimental result.

We estimate the experimental phase boundaries of the intermediate phase $V_{\mathcal{I}}$ and $V_{\mathcal{E}}$ via empirical fit functions [34] to the measured imbalance and expansion, which are shown as black solid lines in Figs. 3(a)–3(c). Here, $V_{\mathcal{I}}$ denotes the lower phase boundary between the extended and the intermediate phase, which is marked by the detuning lattice depth where the imbalance first becomes finite. The upper phase boundary between the intermediate and localized phase $V_{\mathcal{E}}$ is at the depth of the detuning lattice where the expansion vanishes. The theoretical phase boundaries are estimated via the detuning strengths where the imbalance (or edge density) first crosses a value of 0.015, which is just above the noise floor of the simulations. This is the same method employed in Ref. [25]. The resulting phase diagram is presented in Fig. 4. We find very good agreement between the experimental phase boundaries and the numerical calculations that include averaging over many tubes. A slight trend of the experiment to underestimate $V_{\mathcal{I}}$ can be attributed to finite time effects [34]. The numerical simulations not including the averaging over tubes show a smaller, but still clearly pronounced, intermediate phase (Fig. 4 inset).

The intermediate phase, in which localized and extended states coexist, is most pronounced at low depths of the primary lattice V_p. It shrinks and shifts towards lower detuning lattice depths when the primary lattice depth is increased. In the experiment, the intermediate phase retains a small finite width even for large primary lattice depths. The comparison of numerical simulations with and without averaging over tubes shows that such a measured finite extent of the intermediate phase at, e.g., $V_p = 8E_r^p$ is almost entirely due to averaging over tubes. The intermediate phase in a single tube essentially vanishes for such primary lattice depths. Hence, in this regime, all single-particle states localize at the same critical depth of the detuning lattice with no SPME present, and the system accurately maps onto the Aubry-André model [29]. The results of Fig. 4 suggest that a description by the Aubry-André model is approximately possible beyond primary lattice depths of $V_p > 7E_r^p$, and indeed earlier experimental work on localization in the Aubry-André model has been performed in this regime [28,30].

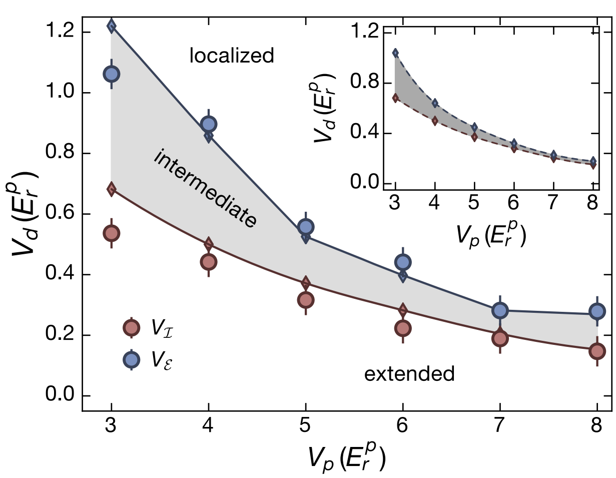

FIG. 4. Phase diagram of the incommensurate lattice model. Boundaries of the intermediate phase (gray) as extracted from the imbalance $\mathcal{I}$ and expansion $\mathcal{E}$ from the experiment (points) and numerics (diamonds and lines) including averaging over tubes. The inset shows the numerical results for the central tube.

Summary and outlook.—We have experimentally investigated the localization properties of a bichromatic incommensurate lattice potential over a large parameter space with noninteracting atoms. We experimentally found an intermediate phase separating the fully extended from the fully localized phase, in very good agreement with numerical simulations. In this intermediate phase, localized and extended states coexist and numerics show that a SPME is present [25]. The intermediate phase vanishes in the tight-binding limit, where the lattice system maps onto the Aubry-André model [29]. An experimental measurement of the critical energy separating extended from localized states would be an interesting goal for future work.

Our Letter presents the first experimental realization of a system with a SPME in one dimension, thus concluding a 30-year-long search for an experimentally realizable model. Adding interactions is readily possible in our setup, opening up research prospects also in the context of many-body localization [37–40], where couplings between localized and delocalized states via interactions might give insights into the question of the existence of a many-body mobility edge. In fact, the possible interplay of the SPME with interaction [41,42] remains the important open future question in this system. There are two closely related questions of fundamental importance in this problem: (1) Does many-body localization persist in the presence of a SPME as it does in the corresponding interacting Aubry-André model [30,38]? (2) Is there a many-body mobility edge in the presence of interactions? We hope to explore both questions experimentally in the future.

The authors thank Xiaopeng Li for discussions. We acknowledge financial support by the European Commission (UQUAM, AQuS) and the Nanosystems Initiative Munich (NIM). Further, this work is supported by Microsoft and the Laboratory for Physical Sciences.

*Corresponding author.
immanuel.bloch@mpq.mpg.de

[1] P. W. Anderson, Absence of diffusion in certain random lattices, Phys. Rev. **109**, 1492 (1958).

[2] E. Abrahams, P. W. Anderson, D. C. Licciardello, and T. V. Ramakrishnan, Scaling Theory of Localization: Absence of Quantum Diffusion in Two Dimensions, Phys. Rev. Lett. **42**, 673 (1979).

[3] P. A. Lee and T. V. Ramakrishnan, Disordered electronic systems, Rev. Mod. Phys. **57**, 287 (1985).

[4] G. Semeghini, M. Landini, P. Castilho, S. Roy, G. Spagnolli, A. Trenkwalder, M. Fattori, M. Inguscio, and G. Modugno, Measurement of the mobility edge for 3D Anderson localization, Nat. Phys. **11**, 554 (2015).

[5] F. Jendrzejewski, A. Bernard, K. Muller, P. Cheinet, V. Josse, M. Piraud, L. Pezze, L. Sanchez-Palencia, A. Aspect, and P. Bouyer, Three-dimensional localization of ultracold atoms in an optical disordered potential, Nat. Phys. **8**, 398 (2012).

[6] W. R. McGehee, S. S. Kondov, W. Xu, J. J. Zirbel, and B. DeMarco, Three-Dimensional Anderson Localization in Variable Scale Disorder, Phys. Rev. Lett. **111**, 145303 (2013).

[7] M. Pasek, G. Orso, and D. Delande, Anderson Localization of Ultracold Atoms: Where is the Mobility Edge?, Phys. Rev. Lett. **118**, 170403 (2017).

[8] F. Delyon, Y. Lévy, and B. Souillard, Anderson localization for one- and quasi-one-dimensional systems, J. Stat. Phys. **41**, 375 (1985).

[9] J. Billy, V. Josse, Z. Zuo, A. Bernard, B. Hambrecht, P. Lugan, D. Clement, L. Sanchez-Palencia, P. Bouyer, and A. Aspect, Direct observation of Anderson localization of matter waves in a controlled disorder, Nature (London) **453**, 891 (2008).

[10] P. Lugan, A. Aspect, L. Sanchez-Palencia, D. Delande, B. Grémaud, C. A. Müller, and C. Miniatura, One-dimensional Anderson localization in certain correlated random potentials, Phys. Rev. A **80**, 023605 (2009).

[11] S. Das Sarma, A. Kobayashi, and R. E. Prange, Proposed Experimental Realization of Anderson Localization in Random and Incommensurate Artificially Layered Systems, Phys. Rev. Lett. **56**, 1280 (1986).

[12] S. Das Sarma, S. He, and X. C. Xie, Mobility Edge in a Model One-Dimensional Potential, Phys. Rev. Lett. **61**, 2144 (1988).

[13] D. J. Thouless, Localization by a Potential with Slowly Varying Period, Phys. Rev. Lett. **61**, 2141 (1988).

[14] S. Das Sarma, S. He, and X. C. Xie, Localization, mobility edges, and metal-insulator transition in a class of one-dimensional slowly varying deterministic potentials, Phys. Rev. B **41**, 5544 (1990).

[15] J. Biddle and S. Das Sarma, Predicted Mobility Edges in One-Dimensional Incommensurate Optical Lattices: An Exactly Solvable Model of Anderson Localization, Phys. Rev. Lett. **104**, 070601 (2010).

[16] J. Biddle, D. J. Priour, B. Wang, and S. Das Sarma, Localization in one-dimensional lattices with non-nearest-neighbor hopping: Generalized Anderson and Aubry-André models, Phys. Rev. B **83**, 075105 (2011).

[17] S. Ganeshan, J. H. Pixley, and S. Das Sarma, Nearest Neighbor Tight Binding Models with an Exact Mobility Edge in One Dimension, Phys. Rev. Lett. **114**, 146601 (2015).

[18] M. Johansson and R. Riklund, Self-dual model for one-dimensional incommensurate crystals including next-nearest-neighbor hopping, and its relation to the Hofstadter model, Phys. Rev. B **43**, 13468 (1991).

[19] M. L. Sun, G. Wang, N. B. Li, and T. Nakayama, Localization-delocalization transition in self-dual quasiperiodic lattices, Europhys. Lett. **110**, 57003 (2015).

[20] M. Johansson, Comment on Localization-delocalization transition in self-dual quasiperiodic lattices by Sun M. L. et al., Europhys. Lett. **112**, 17002 (2015).

[21] A. Purkayastha, A. Dhar, and M. Kulkarni, Non-equilibrium phase diagram of a 1D quasiperiodic system with a single-particle mobility edge, Phys. Rev. B **96**, 180204 (2017).

[22] L. Gong, Y. Feng, and Y. Ding, Anderson localization in one-dimensional quasiperiodic lattice models with nearest- and next-nearest-neighbor hopping, Phys. Lett. A **381**, 588 (2017).

[23] S. Gopalakrishnan, Self-dual quasiperiodic systems with power-law hopping, Phys. Rev. B **96**, 054202 (2017).

[24] D. J. Boers, B. Goedeke, D. Hinrichs, and M. Holthaus, Mobility edges in bichromatic optical lattices, Phys. Rev. A **75**, 063404 (2007).

[25] X. Li, X. Li, and S. Das Sarma, Mobility edges in one-dimensional bichromatic incommensurate potentials, Phys. Rev. B **96**, 085119 (2017).

[26] S. Aubry and G. André, Analyticity breaking and Anderson localization in incommensurate lattices, Ann. Isr. Phys. Soc. **3**, 18 (1980).

[27] L. Fallani, J. E. Lye, V. Guarrera, C. Fort, and M. Inguscio, Ultracold Atoms in a Disordered Crystal of Light: Towards a Bose Glass, Phys. Rev. Lett. **98**, 130404 (2007).

[28] G. Roati, C. D'Errico, L. Fallani, M. Fattori, C. Fort, M. Zaccanti, G. Modugno, M. Modugno, and M. Inguscio, Anderson localization of a non-interacting Bose-Einstein condensate, Nature (London) **453**, 895 (2008).

[29] M. Modugno, Exponential localization in one-dimensional quasiperiodic optical lattices, New J. Phys. **11**, 033023 (2009).

[30] M. Schreiber, S. S. Hodgman, P. Bordia, H. P. Lüschen, M. H. Fischer, R. Vosk, E. Altman, U. Schneider, and I. Bloch, Observation of many-body localization of interacting fermions in a quasirandom optical lattice, Science **349**, 842 (2015).

[31] S. Trotzky, Y-A. Chen, A. Flesch, I. P. McCulloch, U. Schollwöck, J. Eisert, and I. Bloch, Probing the relaxation towards equilibrium in an isolated strongly correlated one-dimensional Bose gas, Nat. Phys. **8**, 325 (2012).

[32] U. Schneider, L. Hackermüller, J. P. Ronzheimer, S. Will, S. Braun, T. Best, I. Bloch, E. Demler, S. Mandt, D. Rasch, and A. Rosch, Fermionic transport and out-of-equilibrium dynamics in a homogeneous Hubbard model with ultracold atoms, Nat. Phys. **8**, 213 (2012).

[33] J. P. Ronzheimer, M. Schreiber, S. Braun, S. S. Hodgman, S. Langer, I. P. McCulloch, F. Heidrich-Meisner, I. Bloch, and U. Schneider, Expansion Dynamics of Interacting Bosons in Homogeneous Lattices in One and Two Dimensions, Phys. Rev. Lett. **110**, 205301 (2013).

[34] See Supplemental Material at http://link.aps.org/supplemental/10.1103/PhysRevLett.120.160404 for additional information.

[35] P. Bordia, H. P. Lüschen, S. S. Hodgman, M. Schreiber, I. Bloch, and U. Schneider, Coupling Identical One-Dimensional Many-Body Localized Systems, Phys. Rev. Lett. **116**, 140401 (2016).

[36] H. P. Lüschen, P. Bordia, S. S. Hodgman, M. Schreiber, S. Sarkar, A. J. Daley, M. H. Fischer, E. Altman, I. Bloch, and U. Schneider, Signatures of Many-Body Localization in a Controlled Open Quantum System, Phys. Rev. X **7**, 011034 (2017).

[37] D. M. Basko, I. L. Aleiner, and B. L. Altschuler, Metal-insulator transition in a weakly interacting many-electron system with localized single-particle states, Ann. Phys. (Amsterdam) **321**, 1126 (2006).

[38] S. Iyer, V. Oganesyan, G. Refael, and D. A. Huse, Many-body localization in a quasiperiodic system, Phys. Rev. B **87**, 134202 (2013).

[39] E. Altman and R. Vosk, Universal dynamics and renormalization in many-body-localized systems, Annu. Rev. Condens. Matter Phys. **6**, 383 (2015).

[40] R. Nandkishore and D. A. Huse, Many-body localization and thermalization in quantum statistical mechanics, Annu. Rev. Condens. Matter Phys. **6**, 15 (2015).

[41] X. Li, S. Ganeshan, J. H. Pixley, and S. Das Sarma, Many-Body Localization and Quantum Nonergodicity in a Model with a Single-Particle Mobility Edge, Phys. Rev. Lett. **115**, 186601 (2015).

[42] R. Modak and S. Mukerjee, Many-Body Localization in the Presence of a Single-Particle Mobility Edge, Phys. Rev. Lett. **115**, 230401 (2015).